Proc. IEEE Computer Vision and Pattern Recognition (CVPR) vol. II, pp. 1861-1868 (2006)

Instant *3D*escatter

Tali Treibitz and Yoav Y. Schechner
Dept. of Electrical Engineering
Technion - Israel Inst. Technology
Haifa 32000, ISRAEL
ttali@tx.technion.ac.il , yoav@ee.technion.ac.il

Abstract

Imaging in scattering media such as fog and water is important but challenging. Images suffer from poor visibility due to backscattering and signal attenuation. Most prior methods for visibility improvement use active illumination scanners (structured and gated), which are slow and cumbersome. On the other hand, natural illumination is inapplicable to dark environments. The current paper counters these deficiencies. We study the formation of images under wide field (non-scanning) artificial illumination. We discovered some characteristics of backscattered light empirically. Based on these, the paper presents a visibility recovery approach which also yields a rough estimate of the 3D scene structure. The method is simple and requires compact hardware, using active wide field polarized illumination. Two images of the scene are instantly taken, with different states of a camera-mounted polarizer. A recovery algorithm then follows. We demonstrate the approach in underwater field experiments.

1 Scattering Media

A wide range of imaging domains exists in scattering media. Several studies [1, 22, 28, 30, 33] improved visibility in such media under natural illumination. However, natural light is in general unavailable in relevant scenarios, as in deep water, pipelines or at night. Moreover, natural illumination may change in time unpredictably [27]. The need to use artificial illumination is therefore obvious. This involves a practical difficulty: the illumination is strongly scattered back towards the camera from particles along the line of sight (LOS), creating *backscatter*, as shown in Fig. 1. The backscatter overwhelms the signal, causing severe loss of visibility. This problem can be alleviated by increasing the baseline between the light source and the camera [11, 34]. This is impossible to do in tight environments such as shipwrecks or pipelines. Moreover, a construction using long strobe arms is cumbersome and less hydrodynamic. In any case, backscatter ultimately overcomes the attenuated signal for far enough objects, no matter how far away the light source is placed. Backscatter can be modulated and then compensated for in image post-processing. Such current methods require acquisition of long image sequences by structured light [14, 16, 23] or time-gating [3, 5, 9, 35, 37]. Such sequences may lengthen the overall acquisition time. Moreover, such systems are very complex and expensive.

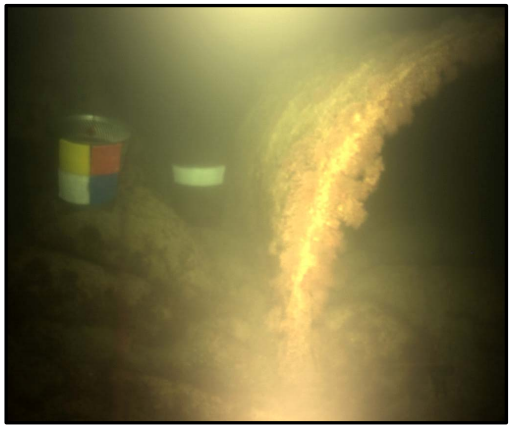

Figure 1. An underwater image taken in the Mediterranean with two artificial light sources. The backscatter greatly degrades visibility, and its nonuniformity creates dynamic range problems.

To counter these problems, we look at widefield (not scanning) illumination with a small (or no) baseline, where the backscatter is modulated by polarization. Preliminary studies [6, 7, 17] indicated that backscatter can be reduced by polarization. However, we go further. By post-processing we remove residual backscatter that is not blocked by optical means. Moreover, a rough estimate of the 3D scene structure may be obtained from the acquired frames. The acquisition setup is a simple modification of instruments used routinely in such media: simply mounting two polarizers, one on the light source and another on the camera. The acquisition process is instantaneous, i.e., requiring only two frames, rather than scanning.

The approach is based on several insights into the image formation process. We show that backscatter and attenuation of artificial illumination can be well approximated by simple closed-form parametric expressions. To incorporate polarization, we have performed empirical polarization measurements in real underwater scenes: in a temperate latitude sea (Mediterranean), a tropical sea (the Red Sea), in a

murky lake (Sea of Galilee) and a swimming pool.

2 Theoretical Background

2.1 Artificial Illumination

Consider a camera in a scattering medium. At pixel (x, y), the measured image $I(x, y)$ is the sum of the object signal $S(x, y)$ and a backscatter component $B(x, y)$,

$$I(x, y) = S(x, y) + B(x, y) \quad . \tag{1}$$

We now detail these components. Let z be the axial distance from the camera of a point in the volume. This scene point is at a distance $R_{\text{source}}(x, y, z)$ from a light source which resides by the camera. The source radiance is L^{source}. The irradiance of the scene point [11] due to this source is

$$I^{\text{source}}(x, y, z) = L^{\text{source}} \frac{\exp[-cR_{\text{source}}(x, y, z)]}{R^2_{\text{source}}(x, y, z)} \quad . \tag{2}$$

Eq. (2) is affected by the medium, which is characterized by an attenuation coefficient c and by the $1/R^2_{\text{source}}$ falloff caused by free space propagation. Here $c = a + b$, where a is the absorption coefficient of the medium and b is its total scattering coefficient. The latter expresses the ability of an infinitesimal medium volume to scatter flux in all directions. Integrating over all solid angles $\mathbf{\Theta}$,

$$b = \int_{\mathbf{\Theta}} b(\mathbf{\Theta}) d\Omega = 2\pi \int_0^{\pi} b\,(\theta) \sin(\theta)\, d\theta \quad , \tag{3}$$

where $\theta \in [0, \pi]$ is the scattering angle relative to the propagation direction [21]. Note that the variables $a, b(\theta)$ and c are all functions of the wavelength λ. The range $\theta \in [0, \pi/2)$ corresponds to *forward scattering*, while $\theta \in [\pi/2, \pi]$ corresponds to *backscattering*.

Since the camera is beside the artificial illumination source, it is backscatter that affects the sensed image most. It is a result of accumulation [11, 19] of all backscattered light along the line of sight (LOS). Any backscattering from a particle in the medium undergoes attenuation in the distance (see Fig. 2)

$$R_{\text{cam}} = \sqrt{(\alpha x)^2 + (\alpha y)^2 + z^2} \tag{4}$$

between that particle and the camera, where $\alpha(z)$ is the camera magnification. Integrating all these scattering incidences,

$$B(x, y) = \int_0^{Z_{\text{obj}}(x,y)} b[\theta(z)] I^{\text{source}}(z) \exp[-cR_{\text{cam}}(z)] dz. \tag{5}$$

The integration stops where an object is encountered in a distance Z_{obj}. Note that θ, I^{source} and R_{cam} all change with z. Moreover, they all depend on (x, y).

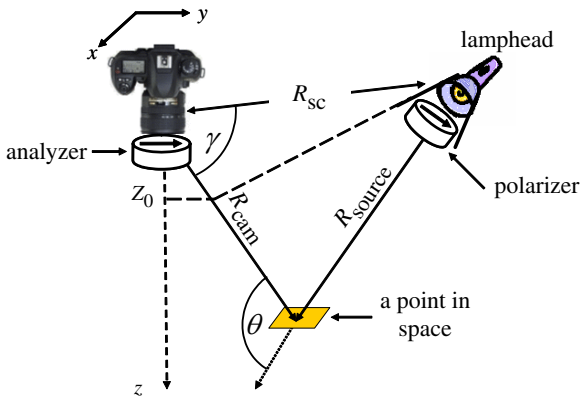

Figure 2. The setup. R_{cam}- distance of a point from the camera; R_{source}- distance of a point from a light source; R_{sc}- baseline; θ- scattering angle; γ- angle between baseline and LOS; x, y- image coordinates; z- axial coordinate; Z_0- axial distance to first intersection of light with the LOS.

2.2 Object Signal

Define $L_{\text{object}}(x, y)$ as the object radiance we would have sensed had no falloff occurred (as if scene irradiance is done by a distant source, with no attenuating media). The object irradiance suffers [11, 19] from falloff[1] as described in Eq. (2). Light reflected from the object then undergoes attenuation along the LOS. We define a falloff function

$$F(x, y) = \frac{e^{-c[R_{\text{source}}(x,y,Z_{\text{obj}}) + R_{\text{cam}}(x,y,Z_{\text{obj}})]}}{R^2_{\text{source}}(x, y, Z_{\text{obj}})} \quad . \tag{6}$$

Hence, the signal originating from the object is

$$S(x, y) = L^{\text{object}}(x, y) F(x, y) \quad . \tag{7}$$

2.3 Active Polarization Imaging

By mounting a polarizer on the light source, we polarize the illumination (see [10] for polarization definitions). This light is then backscattered by particles in the medium. Had the backscattered light been completely polarized, it could have been optically eliminated by a camera-mounted polarizer (an *analyzer*). However, backscattering involves some *depolarization*, i.e., some energy of the light becomes unpolarized, hence cannot be blocked by an analyzer. Nevertheless, a substantial degree of polarization (DOP) is maintained upon backscattering. We exploit this phenomenon.[2]

Once light is backscattered, it propagates through the scattering medium towards the camera. During this propagation, it further depolarizes [32]. This process is complex

[1] Blur due to forward scattering affects image quality less than the other effects [28]. Therefore, we do not handle it in this work.

[2] Polarization aids other computer vision aspects [2, 4, 20, 22, 31, 33].

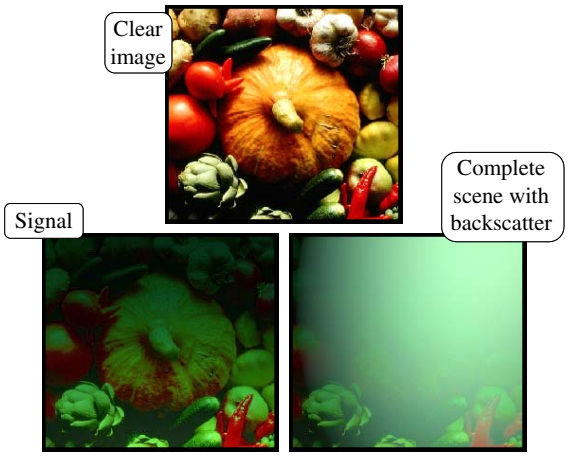

Figure 3. Simulated actively illuminated scene.

and depends on the distribution of particle types and sizes and polarization type [12, 13, 18, 26]. A preliminary empirical study [7] showed that if the illumination is circularly polarized, then a significant improvement in contrast can be achieved optically in water. The bottom line, however, is that this phenomenon is not well modelled yet for most real world media. In particular, we have not found in current literature a clear answer as to which polarization type is preferable in the water environments we worked in, and how depolarization rate correlates with the scattering or attenuation coefficients. Hence we had to take the plunge, literally, and check the matter in-situ.

3 Scene Rendering

To make scene reconstruction tractable, we sought approximations. We obtained this by rendering underwater scenes based on the models of Sec. 2. This enabled us to gauge the importance of various effects and setup parameters, such as camera-illuminator baseline, scene range, medium coefficients, illumination spectrum and angular non-uniformity of the light source.

Rendering relied on the properties of a Nikon D100, a 20mm lens and the spectrum of a 100W Quartz Tungsten Halogen bulb [24]. For example, the simulated source in Fig. 3 is placed 14cm to the upper-right of the camera lens, with its axis parallel to the camera axis. The angular spread and non-uniformity of the source are similar to those of the one we used in experiments. The rest of the parameters were variable. The scene was assigned a distance map, e.g., varying linearly with y in the range 0.5-4.5m.

Fig. 3 shows a clear image L^{object}. Here we used oceanic water characteristics (absorption and scattering specifications) as in [21]. A signal derived from this object is shown as well, next to the corresponding image I. It is clear that backscatter overwhelms the farther regions of the object. Moreover, these rendered images illustrate the non-uniformity of the backscatter and scene illumination caused by the falloff.

4 Assumptions and Approximations

For efficient rendering as well as reconstruction, it is beneficial to make some assumptions and approximations.

• **Depolarization**. As a default, we assume that depolarization due to propagation is not significant, since effective propagation distances are rather short in widefield artificial illumination [34], due to the falloff function (Eq. 6).

• **The object's signal**. We assume[3] that S is unpolarized as explained in [29].

• **Uniform backscatter coefficient**. In the following, we mainly refer to oceanic water. In this environment, according to [15], the function $b(\theta)$ is insensitive to θ at backscatter angles ($\theta \geq \pi/2$). Hence, we denote its typical value as $\tilde{b}$. This simplifies the backscatter integrations.

• **A closed form parametric expression for the backscatter integral**. Before we justify this in general, let us first consider a special case in which the camera-illuminator baseline is very small, relative to the object distance. In this case,

$$R_{\text{source}}(x,y) \simeq R_{\text{cam}}(x,y) \quad . \tag{8}$$

Hence,

$$F_{\text{approx}}(x,y,z) = \frac{\exp[-2cR_{\text{cam}}(x,y,z)]}{R^2_{\text{cam}}(x,y,z)} \quad , \tag{9}$$

and

$$B(x,y) \approx \tilde{b} L^{\text{source}} \int_{Z_0(x,y)}^{Z(x,y)} F_{\text{approx}}(x,y,z)dz \quad . \tag{10}$$

Note that the integration does not start at $z = 0$. The reason is that light from the source does not illuminate the space interfacing with the camera lens. Rather, there is a minimum distance Z_0, at which light rays from the illumination source intersect the LOS.[4] The range $z < Z_0$ is effectively dark, and therefore does not contribute to the backscatter. Note that Z_0 is a function of the pixel coordinate (x, y).

An analytic solution to the integral in Eq. (10) is given as the series

$$\frac{B}{\tilde{b}L^{\text{source}}} \approx \left[-\frac{e^{-2cz}}{z} - 2c\ln z - 2c\sum_{n=1}^{\infty} \frac{(-2cz)^n}{n \cdot n!} \right]_{z=Z_0}^{z=Z} . \tag{11}$$

Now, consider a special case where $Z(x,y) = \infty$, i.e., effectively there is no object in front of the camera at (x, y). Denote the backscatter value there as $B_\infty(x,y)$.

[3] Some studies [38, 39] assume that the signal is polarized, ignoring the backscatter polarization.

[4] If the light cone emitted by the illuminator was sharp, then Z_0 could have been geometrically calculated.

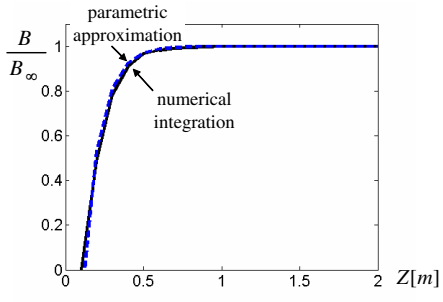

Figure 4. The backscatter given by Eq. (10) as approximated by Eq. (12), with $c = 0.1\ m^{-1}$.

We found in extensive numerical simulations, that Eq. (11) can be well approximated as

$$B \approx B_\infty \{1 - \exp[-k(Z - Z_0)]\} \ , \qquad (12)$$

where k is a parameter that depends only on c and $\tilde{b}$ for a given Z_0. An example is shown in Fig. 4, for a particular setup. Eq. (12) is simple. It has three parameters: an offset Z_0; a slope near Z_0, which is dictated by k, and a saturation value B_∞. We use this approximation in our subsequent derivations.

In general, the setup is more complicated: a light source is *not* coaxial with the camera, it is very *nonuniform* and there are several sources, generally. Hence we simulated the backscatter resulting from such systems being in the medium. Even then, we discovered through simulations that the numerical integration of backscatter *still* follows the approximated model expressed in Eq. (12). The only difference is that the parameters $Z_0,\ k$ and B_∞ vary with (x, y). To conclude, we use Eq. (12) for backscatter caused by a general active illumination system in the medium. To work with the model, however, its parameters need to be determined per pixel. Next, we describe how they can be calibrated in-situ.

Note that [36] simplified the integral in Eq. (5) to a closed form containing values obtained from a precalculated lookup table. This expression is less useful when aiming to invert the process and is very sensitive to noise in the measurements.

Model Calibration

Suppose we have an uncalibrated active illumination system in a medium having unknown characteristics. How can we determine the parameters $Z_0,\ k$ and B_∞ for each pixel (x, y)? Note that $B_\infty(x, y)$ can be easily obtained: rigidly shift the camera/illuminator system, to take a photograph of a void region in the medium (where no object is in sight). The acquired image is simply $B_\infty(x, y)$.

We are left with two unknowns per pixel, $Z_0(x, y)$ and $k(x, y)$. These can be derived by acquiring two calibration frames. A simple procedure is to photograph *within the medium* images of a black board. In one frame, the board is placed at a distance Z_1 from the camera, while in the second one it is placed at a distance Z_2. Since the object is black, the two frames measure only backscatter accumulated up to their respective depths

$$I_i(x, y) = B_\infty(x, y) \left\{1 - e^{-k(x,y)[Z_i - Z_0(x,y)]}\right\}, \qquad (13)$$

for $i \in \{1, 2\}$. These are two nonlinear equations with two unknowns. By setting Z_1 and Z_2 close to the camera, a first order approximation ($[1 - \exp(-\eta)] \simeq \eta$) yields

$$\hat{Z}_0 = \frac{I_1 Z_2 - I_2 Z_1}{I_1 - I_2} \ , \ \hat{k} = \frac{I_1 - I_2}{B_\infty (Z_1 - Z_2)} \ . \qquad (14)$$

Our simulations showed that $\hat{Z}_0$ is insensitive to the color channel. This is expected, since it has a geometric meaning: the intersection of the LOS with the effective boundary of the illumination. We stress that this approximation (Eq. 12) is useful in scene recovery, as detailed in Sec. 5. To demonstrate the effectiveness of the parametric approximation, we performed this parameter calibration, and then used Eq. (12) to render backscatter in scenes. The result is almost indistinguishable from that obtained by numeric integration of backscatter derived from first principles.

5 Scene Reconstruction

We wish to overcome the visibility degradation, and also to estimate a 3D map of the scene. The method has two steps. The first is acquisition using active polarized-illumination and a camera-mounted polarizer. The second is image analysis. We now describe the principles as well as the system we actually used.

5.1 Taking the Plunge

The experiments were done while scuba diving at night in various environments, as described above. To observe color effects in the images, we prepared colorful patch-targets and took them with us. The camera was mounted on a tripod with weights on. To safely sink and float this amount of equipment in a dive, we used a lift bag (Fig. 5).

Other studies have experimented with indoor water tanks, dilluting a fixed substance, usually milk. The particles in milk and other lipid substances are usually homogeneous and symmetric [12, 26] while oceanic particles are heterogeneous [21]. Therefore, we were concerned that polarization experiments done with milk would not represent correctly the properties of the media in the field, e.g., seawater. Thus, we embarked on outdoor dives.

5.2 Image Acquisition

The system setup is depicted in Figs. 2 and 6. *Polarizers* are mounted on the sources while a polarizer is mounted on

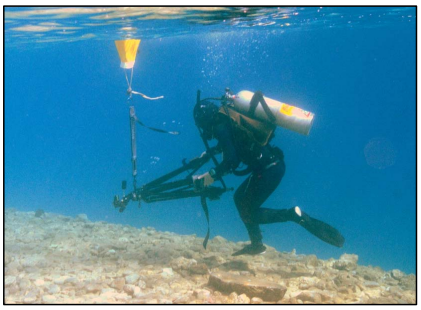

Figure 5. Scuba diving with a lift bag towards night experiments in the Red Sea.

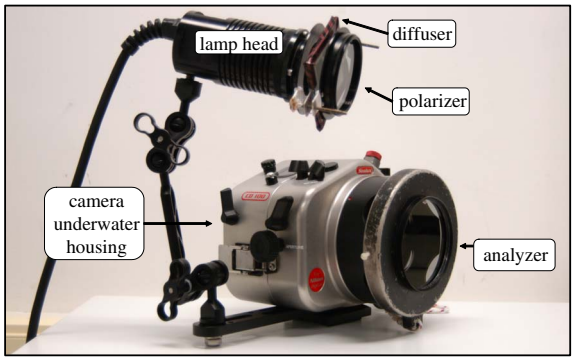

Figure 6. A single-lamphead version of our system.

the camera (*analyzer*). They are either both linear or both circular [7] polarizers. Note that it is more difficult to switch states (handedness) of circular polarization than to switch linear orthogonal states. Anyway, images are taken with the analyzer in two orthogonal polarization states. The first state is chosen to be the one with minimum visible backscatter, denoted $I^{\min}$. The second state has maximum backscatter, denoted $I^{\max}$. We use a Nikon D100 camera, which has a linear response [29]. The camera is placed in a Sealux underwater housing. We also use AquaVideo light sources, with 80W Halogen bulbs. Reasons for this selection are detailed in the Appendix. As described in the following, we often measured a significant DOP of backscatter in experiments. Therefore, sometimes even the single $I_{\min}$ image results in a dramatic improvement.

5.3 Backscatter Removal

Often, substantial backscatter is resistant to optical filtering. Further reduction of backscatter is achieved by post processing $I_{\min}$ and $I_{\max}$. As discussed in Sec. 2.3, the backscatter has a certain DOP, so its contribution varies among the two frames. Since in Sec. 4 the signal is assumed to be unpolarized, the images we take are

$$I^{\min} = S/2 + B^{\min}, \quad I^{\max} = S/2 + B^{\max} \quad , \tag{15}$$

where $B^{\min}$ and $B^{\max}$ are the backscatter intensities in the respective polarization filtered images. Without a polarization analyzer, the image acquired would have been

$$I^{\text{tot}} = I^{\min} + I^{\max} \quad . \tag{16}$$

The DOP of the backscatter is

$$p(x,y) = \frac{B^{\max} - B^{\min}}{B} \quad . \tag{17}$$

If we know $p(x,y)$, then using Eqs. (15,17) the backscatter in every point can be calculated as

$$B(x,y) = \frac{I^{\max}(x,y) - I^{\min}(x,y)}{p(x,y)} \quad . \tag{18}$$

Here we make another assumption:

• **Uniform DOP of backscatter**. In experiments we made in various underwater environments and in different periods, we noticed a surprisingly simple behaviour: the DOP of the accumulated backscatter is practically constant across the FOV[5] despite the angular spread of the illumination and views. Thus $p(x,y) = p$.

We extract the DOP directly from the images. Note that in areas where there is no object, $I^{\text{tot}} = B = B_{\infty}$. Therefore, we can choose an area in the image where no object exists, and then extract the DOP from the image using Eq. (17). Alternatively, it can be taken in the calibration step of $B_{\infty}(x,y)$. Based on p and Eq. (18), we estimate the backscatter and then remove it from the raw image

$$S(x,y) = I^{\text{tot}}(x,y) - B(x,y) \quad . \tag{19}$$

The backscatter removal results in a more uniform brightness, decreasing dynamic range problems. This enables better contrast and brightness range across the FOV.

Fig. 1 shows an unpolarized image taken with our system in the Mediterranean, with sea conditions of approximately 8m visibility. Here we used two light sources placed 10cm above and below the LOS. The estimated DOP in this case was 80%. Fig. 7 shows the result of applying Eqs. (18,19) on the scene shown in Fig. 1. There is a significant improvement of visibility compared to the raw frame. Note the revealed rocks in the upper left and bottom, the sand in the periphery and the distant tube region.

Fig. 8 shows an image taken in the fresh water Sea of Galilee with poor visibility of about 0.5m (which imposed significant inconvenience during the experiment). In this setup we used one light source, which was placed 10cm above the LOS. The resulting circular DOP was 9%. The imaged bucket is of the same size as the one shown in Fig. 7, just much closer. Despite its proximity, its rear edge is not visible in the raw images. In contrast, after applying Eqs. (18,19) to the circular polarization pair, the rear edge is unveiled (though blurred). The darkness above that edge correctly indicates the void above and behind the bucket.

[5] We found it is constant up to $\approx 24^{\circ}$ relative to the optical axis.

Figure 7. Result of our method, corresponding to Fig. 1. [Top] Backscatter removal. [Bottom] Estimated backscatter. **To observe the color effects, please view the paper on the computer monitor.**

5.4 Falloff Estimation

As discussed in Sec. 2.1, the amount of backscatter in each pixel is related to the distance of the corresponding object. The farther it is, the more backscatter accumulates along the LOS. In the previous section, we extracted the backscatter map, which indicates the object distance, i.e., the 3D structure of the scene. Furthermore, having this estimation, we can somewhat compensate for the falloff.

The depth values are derived from Eq. (12):

$$\hat{Z}_{\rm obj}(x,y) = Z_0(x,y) - \left[\ln\left(1 - \frac{B(x,y)}{B_\infty(x,y)}\right)\right] / k(x,y) \ . \tag{20}$$

The parameters $k(x,y)$ and $Z_0(x,y)$ are calibrated as explained in Sec. 4.

One should be aware of the limitation of this approach for 3D recovery. For example, Fig. 4 shows the result of a numeric calculation of $B(z)$ using Eq. (10). In the first half a meter the backscatter increases at a high rate. Therefore, estimating distances in this range can be meaningful. On the other hand, after a distance of about 1m the backscatter saturates. Hence trying to distinguish distances there is fruitless. The effective range can be increase to 2-3m when the baseline or the attenuation coefficient change.

After estimating $\hat{Z}_{\rm obj}(x,y)$ in Eq. (20), it can now be used for estimating the falloff. For this, we need the attenuation coefficient c, which can be evaluated by a transmissiometer. In addition, we need $R_{\rm source}$, which is derived based on *a-priori* knowledge about the system baseline: as in [36], it is sufficient to know camera-light-source baseline $R_{\rm sc}$, and the angle between this source and the LOS, γ (See Fig. 2). Then,

$$R_{\rm source} = \sqrt{R_{\rm sc}^2 + R_{\rm cam}^2 - 2R_{\rm cam}R_{\rm sc}\cos\gamma} \ . \tag{21}$$

The value of $\hat{R}_{\rm cam}$ is estimated by setting $z = Z_{\rm obj}$ in Eq. (4). Then Eq. (21) derives $\hat{R}_{\rm source}$. Using them in Eq. (6), we get the estimated falloff $\hat{F}(x,y)$. The latter can be compensated for (see Eq. 7):

$$\hat{L}_{\rm object}(x,y) = S(x,y)/\hat{F}(x,y) \ . \tag{22}$$

Fig. 9 shows a typical dependence of F on B (both are normalized by their maximal value). We can see that the function is stable and estimation of falloff based on backscatter is well-conditioned. Fig. 10 shows a simulation of the entire recovery method. The image was assigned a non-trivial distance map and artificial noise was added with

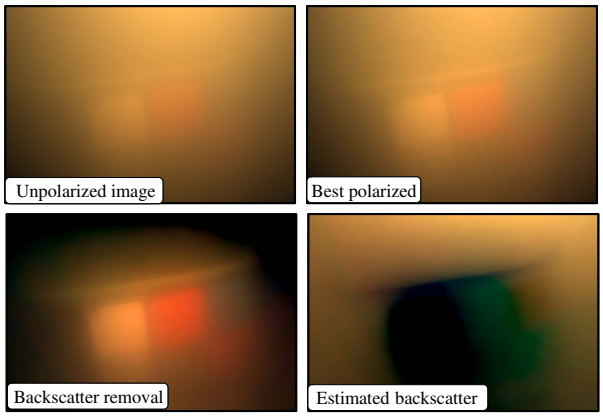

Figure 8. [Top] Images taken in the Sea of Galilee with our system using one light source at the top. [Bottom] Results of our method. **To observe the color effects, please view the paper on the computer monitor.**

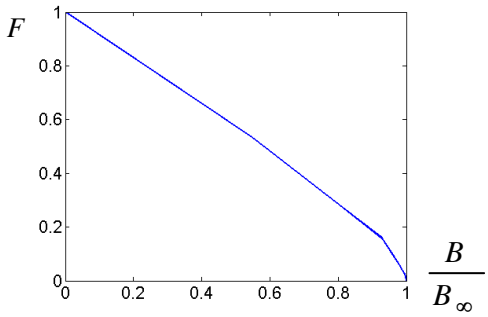

Figure 9. Normalized falloff as a typical function of the backscatter in an arbitrary pixel.

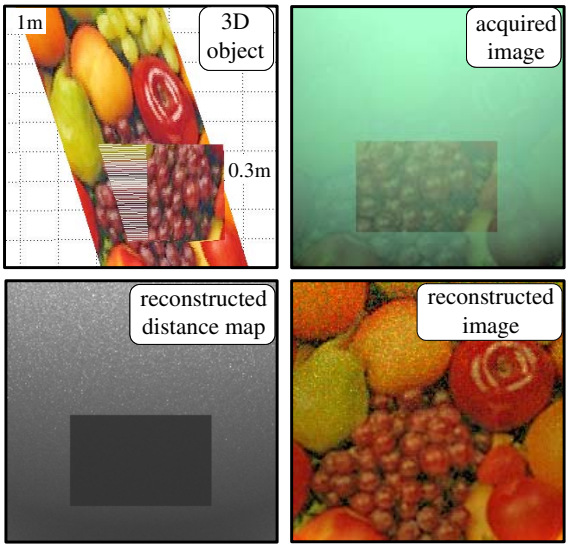

Figure 10. Simulated backscatter removal, 3D recovery and falloff compensation of a noisy object.

standard deviation of 1 grey level (out of 256 in the image). The bottom-right figure shows the image after removal of the estimated backscatter and falloff compensation. While the image is enhanced relative to the acquired image (top right), there is noise amplification in the distant parts. The reconstructed distance map (bottom left) matches the original one (top left).

6 Discussion

Our approach is instant, easy to build and cheap. It is a physics-based enhancement of contrast. The method is general enough and it might work even if not all the assumptions are true, but this requires further exploration. The method may also yield a rough estimate of the 3D scene structure. Note that 3D reconstruction can be done mostly in short ranges, where the backscatter expression still varies rapidly and light still exists with sufficient intensity. On the other hand, visibility recovery is achieved throughout the range of the light source without limit. The practical limit of having less light reaching distant objects is fundamental to all active illumination methods.

We currently work on testing of the calibration method in field experiments. We also started to compare performance of circular polarization to linear one, experimentally and theoretically. Note that circular polarizers are designed for narrow spectra and angles. Widefield and wideband circular polarizers are difficult to construct and are very expensive. In addition, it is worth applying this descatter approach in media other than water.

The method can be combined with spatial/temporal scan methods. Scanners [5, 14] can use lasers which generate polarized light by stimulated emission [10] without loss, while projectors [16, 23] often emit polarized light [25].

Appendix: Illumination Choices

Our system is shown in Fig. 6. It consists of a light source; a diffuser to make the light beam more uniform and widen its spread; a polarizer for the light source; an SLR camera with an underwater housing; and a polarizer mounted on the camera. The considerations for choosing a camera and a housing in conjunction with polarization filtering are detailed in [29]. As for the illumination, we had several requirements, beyond being watertight in the underwater depth, as detailed below.

Stability: We had to avoid uncontrolled illumination fluctuations in this research phase. This has overruled current arc-based flash bulbs, which have $\mathcal{O}(5\%)$ fluctuations [8]. DC incandescent sources are least prone to short-term fluctuations, once their temperature saturates.

Narrow lamphead exit aperture enables fitting high quality filters. This has overruled current large LED clusters or fluorescent bulbs.

Holographic diffusers are used for higher transmission efficiency and smaller diffusing angles.

Sealed diffuser. High efficiency diffusers are either ground/sandblusted glass or holographic. The former become clear (nondiffusing) in water, as their refractive index is nearly matched by water in their concavities. The latter are destroyed in water. Thus, we sealed the diffusers in air spaced windows.

Diffuser before polarizer. Diffusers scramble light, causing depolarization. Lab tests verified a higher illumination DOP when the diffuser is placed between the polarizer and the lamphead, rather than facing the object.

High intensity extends the vision range in the water.

Enough battery power to last for long underwater experiments with fast recharging in field use.

The Aquavideo SuperNova system which we use projects up to 400W by two bulbs. A lower power of 80W lasts for about an hour. It has a 50mm lamphead exit.

Acknowledgements

We thank Dori Yelin, Haim Kermany, Ben Hertzberg, Omer Niv and above all Einav Namer for help in the experimental dives. We thank Nadav Shashar for fruitful discussions and great help. Yoav Schechner is a Landau Fellow - supported by the Taub Foundation, and an Alon Fellow. The work was supported by the Israeli Science Foundation (grant No. 315/04) and by the Ollendorff Center in the Elect. Eng. Dept. at the Technion. Minerva is funded through the BMBF.

References

[1] P. C. Y. Chang, J. C. Flitton, K. I. Hopcraft, E. Jakeman, D. L. Jordan, and J. G. Walker. Improving visibility depth

in passive underwater imaging by use of polarization. *App. Opt.*, 42:2794–2803, 2003.

[2] O. G. Cula, K. J. Dana, D. K. Pai, and D. Wang. Polarization multiplexing for bidirectional imaging. In *Proc. IEEE CVPR*, volume 2, pages 1116–1123, 2005.

[3] S. G. Demos and R. R. Alfano. Temporal gating in highly scattering media by the degree of optical polarization. *Opt. Letters*, 21:161–163, 1996.

[4] H. Farid and E. H. Adelson. Separating reflections and lighting using independent components analysis. In *Proc. IEEE CVPR*, volume 1, pages 262–267, 1999.

[5] G. R. Fournier, D. Bonnier, L. J. Forand, and P. W. Pace. Range-gated underwater laser imaging system. *Opt. Eng*, 32:2185–2190, 1993.

[6] G. C. Giakos. Active backscattered optical polarimetric imaging of scattered targets. In *IEEE Instr. & Measurement Tech. Conf.*, volume 1, pages 430–432, 2004.

[7] G. D. Gilbert and J. C. Pernicka. Improvement of underwater visibility by reduction of backscatter with a circular polarization technique. *App. Opt.*, 6:741–746, 1967.

[8] Hamamatsu. Xenon flash lamps. Catalog TLSX1008E04 (Hamamatsu Photnics K.K., Electron Tube Center), 1998.

[9] S. Harsdorf, R. Reuter, and S. Tönebön. Contrast-enhanced optical imaging of submersible targets. In *Proc. SPIE*, volume 3821, pages 378–383, 1999.

[10] E. Hecht. *Optics*, chapter 8,13. Addison Wesley, 4th edition, 2002.

[11] J. S. Jaffe. Computer modelling and the design of optimal underwater imaging systems. *IEEE J. Oceanic Eng.*, 15:101–111, 1990.

[12] G. Jarry, E. Steimer, V. Damaschini, M. Epifanie, M. Jurczak, and R. Kaiser. Coherence and polarization of light propagating through scattering media and biological tissues. *App. Opt.*, 37:7357–7367, 1998.

[13] G. W. Kattawar and M. J. Raković . Virtues of Mueller Matrix Imaging for Underwater Target Detection. *App. Opt.*, 38:6431–6438, 1999.

[14] D. M. Kocak and F. M. Caimi. The current art of underwater imaging with a glimpse of the past. *MTS Journal*, 39:5–26, 2005.

[15] A. A. Kokhanovsky. *Light Scattering Media Optics*, page 200. Springer, 3rd edition, 2004.

[16] M. Levoy, B. Chen, V. Vaish, M. Horowitz, I. McDowall, and M. Bolas. Synthetic aperture confocal imaging. *ACM TOG*, 23:825–834, 2004.

[17] G. D. Lewis, D. L. Jordan, and P. J. Roberts. Backscattering target detection in a turbid medium by polarization discrimination. *App. Opt.*, 38:3937–3944, 1999.

[18] F. C. MacKintosh, J. X. Zhu, D. J. Pine, and D. A. Weitz. Polarization memory of multiply scattered light. *Phys. Rev. B 40*, 13:9342–9345, 1989.

[19] B. L. McGlamery. A computer model for underwater camera system. In *Proc. SPIE*, volume 208, pages 221–231, 1979.

[20] D. Miyazaki and K. Ikeuchi. Inverse polarization raytracing: estimating surface shape of transparent objects. In *Proc. IEEE CVPR*, volume 2, pages 910–917, 2005.

[21] C. D. Mobley. *Light and Water: Radiative Transfer in Natural Waters*, chapter 3,5. San-Diego: Academic Press, 1994.

[22] E. Namer and Y. Y. Schechner. Advanced visibility improvement based on polarization filtered images. In *Proc. SPIE 5888: Polarization Science and Remote Sensing II*, pages 36–45, 2005.

[23] S. G. Narasimhan, S. K. Nayar, B. Sun, and S. J. Koppal. Structured light in scattering media. In *Proc. IEEE ICCV*, volume 1, pages 420–427, 2005.

[24] Newport. Oriel Light Resources, 2004. p. I-28.

[25] M. Robinson, G. Sharp, and J. Chen. *Polarization Engineering for LCD Projection*. Wiley, 2005.

[26] V. Sankaran, J. T. Walsh, and D. J. Maitland. Comparative study of polarized light propagation in biologic tissues. *J. Biomed. Opt.*, 7:300–306, 2002.

[27] Y. Y. Schechner and N. Karpel. Attenuating natural flicker patterns. In *Proc. MTS/IEEE OCEANS*, pages 1262–1268, 2004.

[28] Y. Y. Schechner and N. Karpel. Clear underwater vision. In *Proc. IEEE CVPR*, volume 1, pages 536–543, 2004.

[29] Y. Y. Schechner and N. Karpel. Recovery of underwater visibility and structure by polarization analysis. *IEEE J. Oceanic Eng.*, 30:570–587, 2005.

[30] Y. Y. Schechner, S. G. Narasimhan, and S. K. Nayar. Polarization-based vision through haze. *App. Opt.*, 42:511–525, 2003.

[31] Y. Y. Schechner, J. Shamir, and N. Kiryati. Polarization and statistical analysis of scenes containing a semi-reflector. *J. Opt. Soc. Amer. A*, 17:276–284, 2000.

[32] N. Shashar, S. Sabbah, and T. W. Cronin. Transmission of linearly polarized light in seawater: implications for polarization signaling. *J. Exper. Biology*, 207:3619–3628, 2004.

[33] S. Shwartz, E. Namer, and Y. Y. Schechner. Blind haze separation. In *Proc. IEEE CVPR*, 2006.

[34] B. Skerry and H. Hall. *Successful Underwater Photography*. New York: Amphoto books, 2002.

[35] M. P. Strand. Imaging model for underwater range-gated imaging systems. In *Proc. SPIE*, volume 1537, pages 151–160, 1991.

[36] B. Sun, R. Ramamoorthi, S. Narasimhan, and S. Nayar. A practical analytic single scattering model for real time rendering. *ACM TOG*, 24:1040–1049, 2005.

[37] B. A. Swartz and J. D. Cummings. Laser range-gated underwater imaging including polarization discrimination. In *Proc. SPIE.*, volume 1537, pages 42–56, 1991.

[38] J. S. Taylor, Jr., and L. B. Wolff. Partial polarization signature results from the field testing of the shallow water real-time imaging polarimeter (SHRIMP). In *Proc. MTS/IEEE OCEANS*, volume 1, pages 107–116, 2001.

[39] J. S. Tyo, M. P. Rowe, E. N. Pugh, and N. Engheta. Target detection in optically scattering media by polarization-difference imaging. *App. Opt.*, 35:1855–1870, 1996.